Dynamic Stall Experiments on Oscillating Airfoils

W.J. McCroskey,* L.W. Carr,† and K.W. McAlister‡
U.S. Army Air Mobility R&D Laboratory, Moffett Field, Calif.

Dynamic stall and unsteady boundary-layer separation have been studied in incompressible flow at moderately large Reynolds numbers. By varying the leading-edge geometry of an NACA 0012 airfoil, three different types of stall were produced, and the vortex shedding phenomenon was found to be the predominant feature of each. In most cases, including the leading-edge stall on the basic NACA 0012 profile, dynamic stall was found *not* to originate with the bursting of a laminar separation bubble, as is commonly believed, but with a breakdown of the turbulent boundary layer.

Nomenclature

c = airfoil chord, m
C_M = pitching-moment coefficient
C_N = normal force coefficient
C_p = pressure coefficient, $(p-p_\infty)/\frac{1}{2}\rho U_\infty^2$
k = reduced frequency, $\omega c/2U_\infty$
M = Mach number
Re = Reynolds number based on c and U_∞
r_o = leading-edge radius, m
t = time, sec
U_∞ = freestream velocity, m/sec
X = chordwise distance from leading edge, normalized by c
α = angle of attack, $\alpha_0+\alpha_1 \sin \omega t$, deg
$\dot{\alpha}$ = rate of change of angle of attack, rad/sec
ω = angular velocity, rad/sec

I. Introduction

THE phenomenon of dynamic stall on airfoils and lifting surfaces in unsteady-flow environments has been studied for many years, both as an important practical problem and as a challenging fundamental one as well. Within the past decade, it has been established[1-7] that a predominant feature of dynamic stall is the shedding of a strong vortex-like disturbance from the leading-edge region. This vortex passes over the upper surface of the airfoil, distorting the chordwise pressure distribution and producing transient forces and moments that are fundamentally different from their static-stall counterparts (as illustrated in Fig. 1). This unique viscous-inviscid interaction is not well understood at present, although it has been proposed[8,9] that the process begins with the sudden bursting of a leading-edge laminar separation bubble. Accordingly, some recent theoretical viscous analyses[8-10] have focused on leading-edge bubble characteristics, while others [1,2,4,11] have modeled the phenomenon with potential vortices that are emitted from the leading-edge after an assumed bubble bursting.

The present experimental investigation is an outgrowth of the oscillating airfoil study described by Martin et al.[5] Although that previous study linked the measured transient pressure distribution to flow visualizations of the vortex shedding and passage over the airfoil, the measurements did not reveal the detailed nature of the boundary-layer separation. Therefore, attention was focused in the present study on these basic questions: When and where on the airfoil does the boundary layer begin to separate, and what is the mechanism that feeds the leading-edge vortex?

Presented as Paper 75-125 at the AIAA 13th Aerospace Sciences Meeting, Pasadena, California, January 20-22, 1975; submitted February 7, 1975; revision received August 21, 1975.

Index categories: Boundary Layers and Convective Heat Transfer-Turbulent; Nonsteady Aerodynamics.

*Research Scientist, Ames Directorate. Associate Fellow, AIAA
†Research Scientist, Ames Directorate. Member AIAA.
‡Research Scientist, Ames Directorate.

This paper describes the most important results that have been obtained from the first phase of the rather comprehensive experiment, including the different types of boundary-layer separation that were observed on different airfoils, the general effects of the vortex shedding phenomenon at different frequencies, and the effect of leading-edge geometry on the normal force and pitching moment coefficients. Additional results and flow visualization photographs were presented in Ref. 12, and more will be published in future reports.

II. Description of Experiment

The basic configuration was the same as that used by Martin et al.[5]: a NACA 0012 airfoil of 1.22 m chord and 2.0 m span mounted vertically in the U.S. Army AMRDL 7×10-ft wind tunnel. The model was oscillated sinusoidally in pitch about the quarter chord. A more complete description of the model and a photograph of the test setup are given in Ref. 5.

A number of leading-edge modifications (illustrated in Fig. 2) were attached to the basic NACA 0012 profile in an attempt to modify the dynamic-stall characteristics by altering the nature of the bubble. The ONERA "0012 a Extension Cambré" airfoil[13] was chosen to study the effects of camber. The ONERA Cambre was also tested at negative incidence, along with two symmetrical extensions that reduced the leading-edge radius, in an attempt to promote stall due to bubble bursting. The leading-edge serrations shown in Fig. 2 were patterned after the configurations that were found to be most effective by Soderman[14] and Schwind and Allen,[15] and were tested to determine their dynamic characteristics.

Boundary-layer trips were applied to the geometrical leading edge of each configuration. Oil-flow visualization under static conditions near stall indicated that the trips promoted transition ahead of laminar separation, thereby eliiminating the leading-edge bubble, in all cases except the sharp leading-edge airfoil. The use of these trips proved to be extremely valuable in identifying which airfoils stalled by the mechanism of bubble bursting and which ones did not.

Instrumentation and Test Techniques

Oil smoke provided valuable flow visualization of the boundary-layer separation and flowfield behavior during dynamic stall. Smoke ports were installed at $X=0$, 0.20, 0.45, 0.70, and 0.90, and small tufts were attached to the model at several chordwise stations. Two high-speed Milliken movie cameras were mounted above the model outside the test section to record the dynamic changes in the smoke layers and tufts.

The static pressure distributions were measured with surface-mounted Kulite miniature pressure transducers, Type YQCH-250-1. The transducer signals were fed into operational amplifier integrating circuits to give outputs

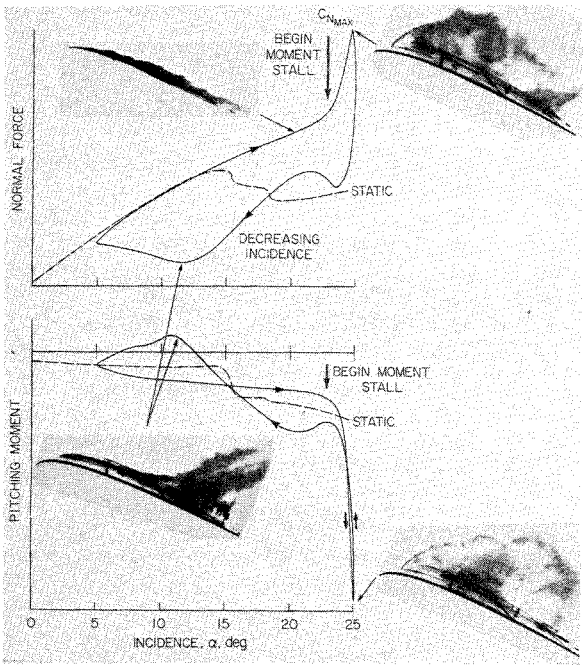

Fig. 1 Normal force and pitching moment on NACA 0012 airfoil during dynamic stall. ($\alpha = 15° + 10°$ sin ωt, $k = \omega c/2U_\infty = 0.15$, Re $= 2.5 \times 10^6$).

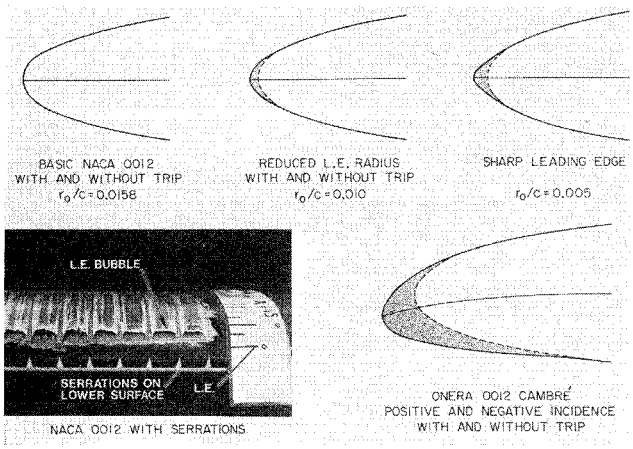

Fig. 2 Variations in leading-edge geometry used in the experiment.

proportional to instantaneous normal force and pitching moment. Some representative oscillograph traces taken during the test are shown in Fig. 3.

Considerable boundary-layer information was obtained with conventional hot-wire anemometers, in addition to single-and dual-element heated-film skin-friction gages, special reverse-flow hot-wire probes that were designed to detect changes in flow direction, and miniature pitot-static pressure tubes facing both upstream and downstream. It should be mentioned that although the response of a single hot wire never becomes negative, a minimum is reached as the flow direction in the boundary layer changes sign, and this characteristic can be used to infer flow reversal. Also, certain boundary-layer behavior could normally be inferred from the qualitative dynamic response of the wires. In Fig. 3, for example, a sharp break in the hot-wire signal near the leading edge at $X = 0.05$, at the point marked R, heralds an abrupt breakdown of the flow, and this signal is labeled Type I in subsequent figures and discussions. The signal at $X = 0.45$, Type II, drops to a distinct minimum value as the flow reverses, although the flow breakdown appears much less abrupt than for Type I. Near the trailing edge, the approach to reversed

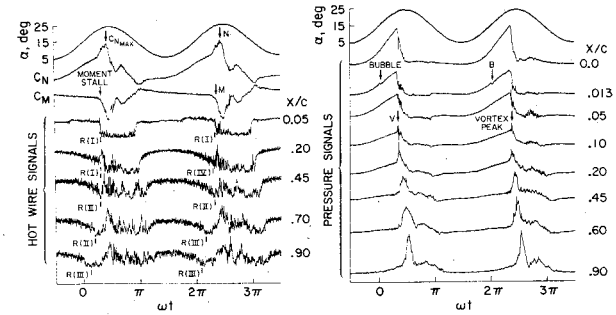

Fig. 3 Representative oscillograph traces during dynamic stall on NACA 0012. Points R indicate flow reversal or separation: Type I-abrupt separation; Type II-onset of flow reversal at distinct minimum; Type III-incipient flow reversal during broad minimum; Type IV-large fluctuations or irregular variations from cycle to cycle.

flow was much more gradual, and a distinct instant of flow reversal was more difficult to ascertain in the presence of random turbulent fluctuations. This case, Type III, was defined on the basis of the first fluctuation to zero, akin to the "intermittent turbulent separation" definition of Sandborn and Kline[16] for nominally steady flows. It seems to precede true flow reversal in any average sense, and this event was always found to precede static-pressure or pitot-pressure disturbances that accompanied boundary-layer separation. It also occurred earlier near the wall than in the outer regions of the boundary layer.

In some cases, large irregular fluctuations, such as in the second cycle in Fig. 3 at $X = 0.20$, or major variations from one cycle to the next, made it difficult to define flow reversal precisely or even to define a specific category of signal. However, close examination of the time history would usually reveal some fairly distinct change in the character of the signal that seemed symptomatic of either flow reversal or boundary-layer separation, and this type of signals was called Type IV. In any case, the combined information from the hot wires and other measurements gives an indication of the initial boundary-layer separation characteristics that lead to the vortex shedding phenomenon.

Test Conditions

The upper part of Table 1 indicates the various parameters that are thought to influence dynamic stall and the extent to which these parameters were varied during the test program. Most of the data were acquired at a freestream velocity of 30.5 m/sec, or Re $\simeq 2.5 \times 10^6$, and with $\alpha = 15° + 10° \sin \omega t$. In this case, ω was varied from 0 to 1.94 Hz, giving a maximum reduced frequency of $k = 0.25$. The amplitude of the oscillation α_I was varied from 6° to 14 ° at a constant value of $\dot{\alpha}c/U_\infty \simeq 0.05$, corresponding to the value of $k = 0.15$ in the standard $15° \pm 10°$ case.

At the lowest frequencies, the oscillating model caused substantial variations in the upstream tunnel flow, and tuft and smoke-flow visualization indicated large three-dimensional interactions between the model and the tunnel-wall boundary layers. However, these adverse effects diminished rapidly with increasing k, and they could hardly be detected for $k \geq 0.15$. The freestream turbulence level for these conditions was normally about 0.7%.

III. Results and Discussion

The lower part of Table 1 indicates the variations in the stall characteristics that were observed as the test parameters were varied one at a time. The general vortex-shedding phenomenon, which has been documented in Refs. 1-7 over very wide ranges of Reynolds number, was observed for all the airfoil shapes tested in the present investigation, whether the boundary-layer trip was used or not. Thus, it appears that

Table 1 Variations in test conditions and their influence on dynamic stall

	$Re \times 10^{-6}$	α_1	k	Geometry	M	α_0
Variation	1.0-3.5	6°-14°	0-0.25	Leading edge (Fig. 2)	0.04-0.13	15°
Effect on vortex shedding	Negligible	Major in isolated cases	Small	Moderate	Not studied	Not studied
Effect on C_N, C_M	Small	Major in isolated cases	Major	Major		
Boundary-layer separation	Small	Moderate	Major	Major		

this distinguishing feature of dynamic stall is essentially independent of Reynolds number, airfoil geometry, and state of the boundary layer. However, major differences were observed in the stall angle, in the time history of the aerodynamic forces and moments, and in the detailed nature of the boundary-layer separation leading up to dynamic stall. As shown in the following sections, these differences were found to depend upon reduced frequency, upon whether the airfoil stalled due to the bursting of the leading-edge laminar separation bubble, and upon whether the airfoil stalled well before α_{max}, or near the top of the cycle where $\dot{\alpha} \approx 0$.

Dynamic Stall on NACA 0012 Airfoil

The vortex-shedding process involves a series of distinct events, shown in different ways in Figs. 1, 3, and 4 for the standard case of $k=0.15$ and $\alpha = 15° + 10° \sin \omega t$. First, the static-stall angle is exceeded, with the boundary layer remaining thin and showing no evidence of separation of flow reversal. At $\alpha \simeq 19°$ to 20° for these conditions, Type-III flow reversal appears at the rearmost hot wire, the boundary layer on the rear portion of the airfoil begins to thicken rapidly, large eddies give a wavy character to the smoke in the boundary layer, and a region of flow that is virtually quiescent in the mean begins to form near the surface downstream of $X \gtrsim 0.70$. The onset of major changes in the character of the smoke within the boundary layer defines the lower part of the flow visualization boundary in Fig. 4 between attached and fully separated flow.

The region of highly disturbed boundary-layer flow progresses upstream with increasing incidence, or time, to somewhere in the vicinity of $X=0.3$. Small disturbances begin to appear in the surface pressure distribution slightly after incipient flow reversal is indicated by the hot wires; this is indicated by the open circles in Fig. 4. Generally, the tufts and smoke jets from the rear ports begin to reverse direction and move upstream somewhat later than when the first disturbances to the static pressure appear, and this defines the upper part of the flow visualization boundary shown in Fig. 4.

At $\omega t \simeq 1.0$, or $\alpha \simeq 23.4°$, the boundary-layer flow on the front of the airfoil abruptly breaks down catastrophically, or separates. As near as can be determined from the hot-wire and static-pressure data, this event occurs simultaneously in the turbulent flow from $X=0.30$ almost to the leading edge, although the boundary flow in the immediate vicinity of the laminar leading-edge bubble does not completely separate until slightly later. When this abrupt separation occurs, the static suction at $X=0.10$ begins to rise, indicating the initial formation of the vortex. As this vortex begins to form and move downstream, the magnitude of the reversed velocity near the surface of the model increases. The solid symbols in Fig. 4 indicate the negative peak in static pressure and a major peak in the reverse velocity as measured by the hot wires and rearward-facing pitot tubes; these indicate that the vortex is traveling at approximately 35-40% of freestream velocity.

The sudden change in the pressure distribution on the airfoil that occurs at $\omega t \simeq 1.0$ causes the aerodynamic pitching moment to change drastically. This is called moment stall, and is analogous to the change in C_M that occurs in static stall. It is interesting to note that, while C_M exhibits stall-like behavior, the normal force first changes in a sense opposite to what is ordinarily encountered in stall. That is, C_N begins to rise *faster* with increasing incidence than before. This behavior continues until a maximum in C_N is reached when the vortex is approximately at midchord, and $-C_{M_{max}}$ occurs later still, at $\omega t \simeq 0.47\pi$, or just before maximum incidence. As the vortex passes off the trailing edge at $\omega t \simeq 0.55\pi$, C_N continues to decrease and C_M increases rapidly to values more representative of static stall.

At $\omega t \simeq 0.7\pi$, a second vortexlike disturbance begins to form somewhat ahead of midchord and then move downstream. This produces relatively small secondary peaks in C_N and C_M during this part of the downstroke. During this period and continuing until the final reattachment process starts at $\omega t \simeq 0.95\pi$, flow visualization indicates that the flow in the vicinity of the leading edge alternately reattaches and reseparates, although this is not generally evident from the hot-wire and pressure transducer signals. The reattachment process over the rest of the airfoil is rather interesting and complex, as the photograph in Fig. 1 shows, and it proceeds downstream at approximately 25-35% of the freestream velocity. The hysteresis in C_N and C_M is quite pronounced and, although the boundary-layer flow reattaches all the way to the trailing edge well before $\omega t = 3\pi/2$, the aerodynamic forces and moments do not return to their unstalled values until the airfoil passes through minimum incidence and starts the next upstroke.

The preceding results and discussion are qualitatively representative of a wide range of unsteady conditions. Figures 5-7 show the hot-wire flow reversal and force and moment results for a range of reduced frequencies, and the data indicate a systematic delay in the onset of dynamic stall with increasing frequency. Significant hysteresis in the forces, moments, and boundary-layer separation and reattachment were observed for k as low as 0.004, but the case of $k=0.05$

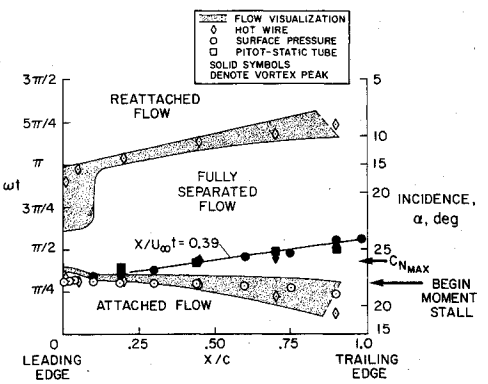

Fig. 4 Sequence of dynamic-stall events on NACA 0012 airfoil at $k=0.15$.

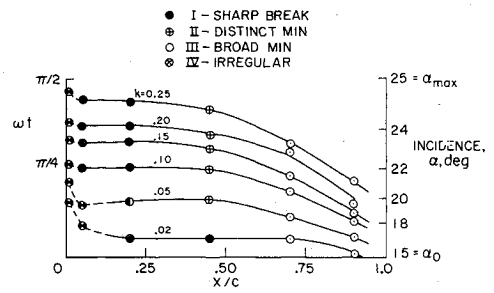

Fig. 5 Hot-wire measurements of boundary-layer flow reversal on NACA 0012 airfoil (Signal types defined in Fig. 3) ($\alpha = 15° + 10°\sin \omega t$, $Re = 2.5 \times 10^6$).

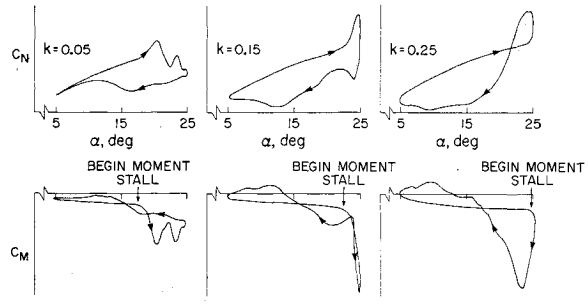

Fig. 6 Variation of normal force and pitching moment with reduced frequency.

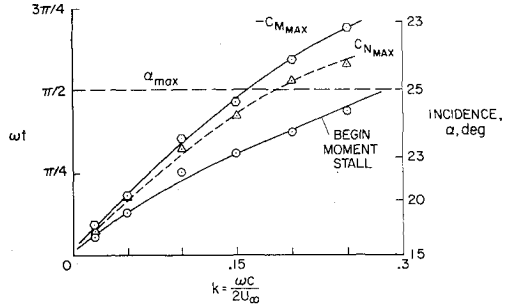

Fig. 7 Variation of force and moment events with reduced frequency for NACA 0012 airfoil ($\alpha = 15° + 10°$ sin ωt, $Re = 2.5 \times 16^6$).

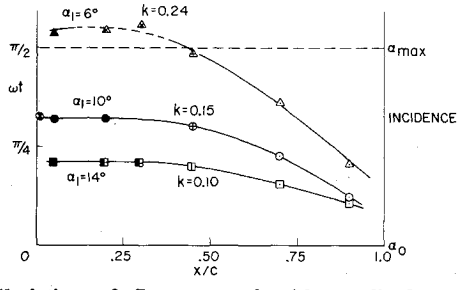

Fig. 8 Variation of flow reversal with amplitude at constant maximum pitch rate for NACA 0012 airfoil ($\alpha = 15° + \alpha_1 \sin \omega t$, $(\dot{\alpha}c/U_\infty)_{max} = 0.05$).

seems to mark the onset of the most salient features of dynamic stall, as already described.

The primary effect of varying the frequency is to vary the phase within the cycle at which the various boundary-layer, vortex shedding, and stall events occur. As a result, the boundary-layer measurements at each frequency (shown in Fig. 5) exhibit the same rear-to-front progression of flow reversal, followed by abrupt separation over the front portion of the airfoil; but these processes occur at successively later times as k increases.

On the other hand, the force and moment data, plotted vs incidence in Fig. 6, vary considerably with k. The vortex shedding phenomenon is not fundamentally different, but both its strength and its phase depend upon reduced frequency. The latter is especially evident in Fig. 7. At $k = 0.05$, moment stall and lift stall occur well before α_{max}, and a subsequent secondary vortex is evident in Fig. 6 during the upstroke. At $k = 0.25$, however, the shedding of the primary vortex occurs near the top of the cycle, as $\dot{\alpha}$ approaches zero. The subsequent delay in $C_{N_{max}}$ until $\omega t > \pi/2$ causes a significant secondary loop in the $C_N - \alpha$ curve at this frequency.

Figures 8 and 9 show the effect of varying the amplitude and frequency simultaneously in such a way as to keep the maximum pitch rate constant. In a qualitative sense, these results are similar to the results shown in Figs. 5 and 6, in which only the frequency was varied. An important exception is the incomplete stall on the ONERA Cambre airfoil at low amplitude and high frequency; this point is deferred to the later section on trailing edge stall.

No influence of Reynolds number was detected over the range $2 \times 10^6 \leq Re \leq 3.5 \times 10^6$. Stall occurred somewhat earlier for $Re \leq 1.5 \times 10^6$ than at the higher values, and the rear-to-front progression of flow reversal was slightly more gradual. However, the nature of the stall characteristics was unchanged over the entire range of Reynolds number.

NACA 0012 with Leading-Edge Modifications

The existence of a distinct leading-edge laminar separation bubble on the basic NACA 0012 airfoil could always be inferred from the hotwire and pressure-transducer signals and, in the static case, from oil-flow visualization. At high incidence, i.e., $\alpha \gtrsim 14°$, the bubble was located very near the leading edge, upstream of $X = 0.007$. However, the initial breakdown of the flow into a type of leading-edge stall always seemed to occur as an abrupt turbulent separation downstream of the bubble location, both statically and dynamically. This circumstance prompted the following leading-edge modifications that were designed specifically to alter the characteristics of the bubble.

First, a boundary-layer trip was employed at $X = 0$ to eliminate the leading-edge laminar separation bubble by promoting transition to turbulence ahead of the bubble. Flow-reversal measurements are shown in Fig. 10 for the standard flow conditions. The Type-III flow reversal on the rear of the airfoil was virtually unaffected, but the breakdown of the leading-edge flow began earlier than in the case without the trip. The onset of stall was more irregular, complex, and ill-defined, and for $k \geq 0.05$, there seemed to be a tendency for the boundary-layer flow between $X = 0.05$ and 0.20 to break down slightly before the flow ar midchord. Also, it should be mentioned that a vortex peak first appeared in the static pressure at $X = 0.05$ for $k \geq 0.05$, whereas this was only observed for $X \geq 0.10$ without the trip, as indicated in Fig. 3. However, the basic stall characteristics and the force and moment data were essentially unchanged.

Next, a leading-edge extension that reduced the leading-edge radius from $0.0158c$ to $0.010c$ (as shown in Fig. 2) was added in an attempt to promote bubble bursting. According to the stall-classification criteria of Gault,[17] this modification should have exhibited even stronger leading-edge stall than the basic 0012 airfoil. Indeed, the static stall characteristics were more abrupt and stall began at a slightly lower incidence. However, the hot-wire measurements of flow reversal did not indicate bubble bursting. In fact, the data at $k = 0.15$ and $Re = 2 \times 10^6$ in Fig. 10 almost coincide with those of the tripped NACA 0012, with flow reversal at $X = 0.20$ preceding the events at $X = 0.05$.

The final configuration in this group is the NACA 0012 airfoil with large-scale serrations. Although such serrations did interact to some extent with the bubble (as Fig. 2 shows), the favorable effects reported by Soderman[14] and Schwind and Allen[15] for other airfoils were not realized. The hot-wire and

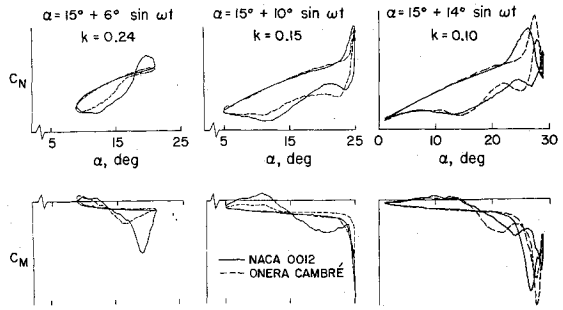

Fig. 9 Force and moment characteristics on NACA 0012 and ONERA Cambre airfoils at $(\dot{\alpha}c/U_\infty)_{max} = 0.05$.

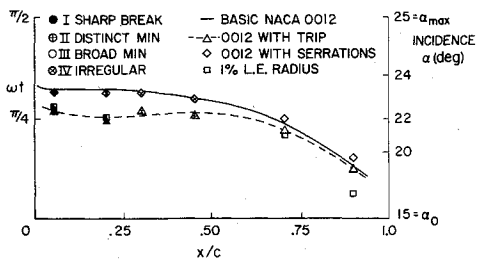

Fig. 10 Flow-reversal measurements on airfoil configurations with similar stall characteristics ($\alpha = 15° + 10°\sin \omega t$, $k = \omega c/2U_\infty = 0.15$).

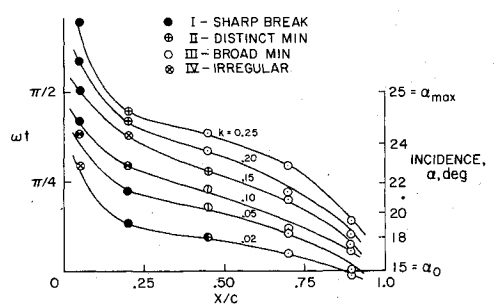

Fig. 11 Flow-reversal measurements during dynamic stall on ONERA Cambre airfoil.

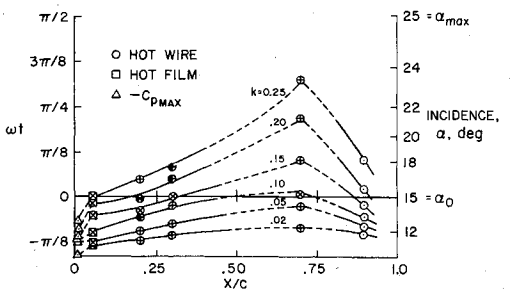

Fig. 12 Flow reversal following bubble bursting on sharp leading-edge airfoil (signal types defined in Figs. 3 and 5).

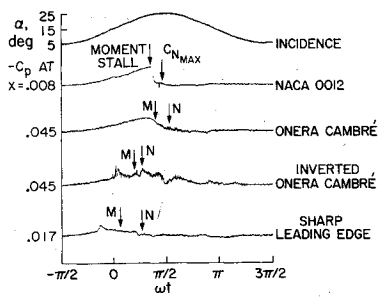

Fig. 13 Variation in static pressure near leading edge on airfoils with different dynamic-stall characteristics ($\alpha = 15° + 10°\sin \omega t$, $k = 0.15$, $Re = 2.5 \times 10^6$).

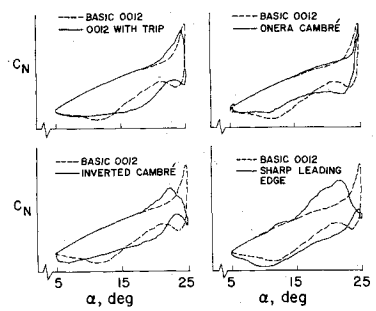

Fig. 14 Comparison of normal force on airfoils with different stall characteristics ($\alpha = 15° + 10°\sin \omega t$, $k = 0.15$, $Re = 2.5 \times 10^6$).

normal-force data were virtually identical to those of the basic NACA 0012. Similar negative results were obtained over the entire frequency range and at $Re = 1.5 \times 10^6$ and 3.5×10^6.

Trailing-Edge Stall on the Cambered Airfoil

Whereas the basic NACA 0012 airfoil and the modifications described in the preceding section appeared to share the common characteristic of stalling by abrupt turbulent separation over the front portion of the airfoil, the ONERA Cambre profile displayed a more classical, relatively gradual, trailing-edge type of stall. Flow-reversal data are shown in Fig. 11 for the standard values of amplitude and Reynolds number considered previously. The contrast with all of the previous cases is striking. Over the entire range of reduced frequencies, flow reversal proceeds progressively from the trailing edge forward to the leading-edge region, and the laminar separation bubble remained intact well beyond stall. An interesting feature of this trailing-edge-stall case is that the shed- vortex disturbance seemed to originate farther downstream than in the previous examples. However, its convection over the airfoil affects the pressure distribution almost the same as before, as shown by the force and moment data in dashed lines in Fig. 9.

In all cases, the onset of stall was found to be delayed relative to the basic 0012 airfoil. For the case $\alpha = 15° + 10°\sin \omega t$ and $k = 0.15$, moment stall begins and $\partial C_N/\partial\alpha$ starts to exceed 2π at $\omega t \simeq 1.1$, or approximately when flow reversal approaches the hot wire at $X = 0.20$. The effects of the primary vortex seem less severe, especially with regard to the maximum negative value of C_M in Fig. 9, and seem to persist for a shorter period of time than those on the 0012. The final reattachment is very similar to that on the basic 0012 airfoil.

For the cases $\alpha = 15° + 6°\sin \omega t$ at $k = 0.20$ and 0.24, the boundary-layer separation never reached the leading edge of the ONERA Cambre airfoil.[12] Accordingly, vortex shedding and the usual vortex-induced behavior of C_N and C_M were not observed in these cases. This exceptional behavior was not found on any other airfoil, nor under any other conditions. However, it should be mentioned that such behavior might be encountered in some practical applications, such as a helicopter just beginning to penetrate into retreating blade stall. Also, it would seem that this case might be more amenable to analysis in the near future, since the separation is relatively gradual, and the stall is less severe.

Bubble Bursting on Two Airfoils

The only airfoils which showed clear indications of stall due to the mechanism of bubble bursting were the sharp-leading-edge modification with $r_0/c = 0.005$ and the ONERA Cambre airfoil inverted, i.e., at negative incidence $\alpha = -15° - 10°\sin$

ωt. Oil-flow visualization revealed a rather elongated bubble of length approximately $0.05c$ at $\alpha = 10°$ on the sharp-leading-edge model, compared with about $0.010c$ on the inverted ONERA profile and about $0.008c$ on the basic NACA 0012. This bubble seened to elongate somewhat before collapsing at $\alpha \simeq 13°$ and, as a result, the static stall characteristics seemed to resemble a modified form of thin airfoil or long bubble stall. However, static stall was more abrupt on the inverted ONERA Cambre airfoil than on any other configuration tested.

In the dynamic cases of both airfoils, smoke and tuft visualization revealed that the boundary layer separated near the leading edge and the primary vortex formed *before* separation had occurred at midchord, in marked contrast with all other configurations. Figure 12 shows the hotwire and heated-film skin-friction gage indications of flow reversal on the sharp-leading-edge model, where the front-to-rear progression of the breakdown of the boundary-layer flow is clearly evident. Another difference is illustrated in Fig. 13, which shows the response of one of the leading-edge pressure transducers for all three types of stall. The peculiar peaks in pressure on the sharp-leading-edge and inverted-Cambre profiles seem to indicate the bursting of the leading-edge separation bubble, and this occurs well before the flow separates downstream of this point. Figure 14 shows the considerably different behavior in normal force and pitching moment.

Additional Discussion of Leading-Edge Stall

Based largely on the static stall classification studies of Gault, et at.[17,18] the abrupt stalling characteristics of the NACA 0012 airfoil at $Re \gtrsim 10^6$ have generally been interpreted to be caused by leading-edge bubble bursting. However, the present data indicate that dynamic leading-edge stall on this airfoil is due to abrupt turbulent separation downstream of the bubble, and this would indicate that the vortex is initially fed its vorticity from the turbulent flow.

Some interesting inferences concerning the mechanisms of leading-edge stall can be drawn from other investigations of static stall. For example, Gregory and O'Reilly[19] reported static behavior at $Re = 2.9 \times 10^6$ that remained essentially unchanged in certain instances when the bubble disappeared, and this led them to suggest that the bubble might not play a crucial role in the stall process. Also, in a recent study of bubble characteristics on a special model with an elliptical leading edge, Ridder[20] observed a change from bubble bursting at low Reynolds number to what appears to have been abrupt turbulent separation at high Reynolds numbers, comparable to the present experiment. Ridder also indicated that, at high Reynolds number and above a certain incidence, the bubble would tend to contract in length with increasing incidence, thereby becoming more lightly loaded and presumably more resistant to bursting.

Finally, in publications that generally seem to have been overlooked in recent years, Wallis[21] put forth an alternative explanation for leading-edge stall; and Evans and Mort[22] tentatively concluded that the NACA 0012, along with several other standard NACA airfoils, behaved more in accord with the Wallis hypothesis that leading-edge stall begins with an unstable turbulent separation a short distance downstream of the bubble reattachment point. This turbulent separation point is then thought to move forward rapidly with increasing incidence until it reaches the bubble, thereby causing an abrupt breakdown of the flowfield. A more detailed analysis of the present hot-wire data has not yet proceeded far enough to verify or disprove Wallis' ideas, although the leading-edge measurements seemed to indicate that vortex shedding and stall began slightly before flow reversal had reached the rear of the bubble in most dynamic cases. What can be concluded, however, is that Evans and Mort were correct in contending that leading-edge stall can arise *either* due to bubble bursting *or* due to abrupt turbulent separation. Both types of flow breakdown were observed in the experiment, and the two are distinctly different.

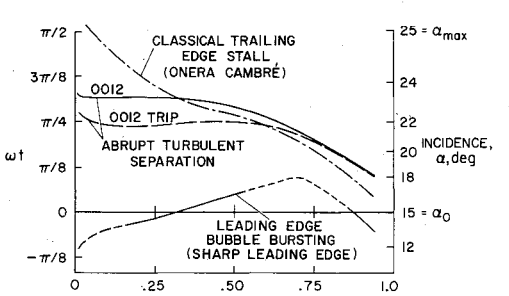

Fig. 15 Summary of flow-reversal measurements on airfoils with different stall characteristics ($\alpha = 15° + 10° \sin \omega t$, $k = 0.15$, $Re = 2.5 \times 10^6$).

IV. Conclusions

Figures 13-15 summarize the results for the three different types of boundary-layer separation that were observed in this experimental investigation of dynamic stall on oscillating airfoils; 1) trailing-edge stall developing from a relatively gradual progression of boundary-layer flow reversal and separation, from the trailing edge toward the leading edge; 2) leading-edge stall caused by an abrupt breakdown of the turbulent flow on the forward portion of the airfoil, following an initial progression of flow reversal from the trailing edge, and 3) two forms of leading-edge stall due to the abrupt bursting of a leading-edge laminar separation bubble. The most important result of the experiment is that leading-edge bubble bursting is much more of a special case than had been commonly assumed heretofore. In the important case of dynamic stall on the NACA 0012 airfoil, the shed vortex appears to be fed its initial vorticity by the abrupt, unsteady separation of the turbulent boundary layer, not the laminar bubble.

Regardless of the type of boundary-layer separation, the main difference between static and dynamic stall is the vortex-shedding phenomenon. Provided the flow separates over most or all of the upper surface of the airfoil, a vortex-like disturbance develops and passes over the airfoil at a convection velocity on the order of ⅓ to ½ of U_∞. The transient aerodynamic forces and moments that are produced are considerably larger and different in nature from their steady-state counterparts. An exception was noted in cases where trailing-edge stall did not penetrate all the way to the leading edge during any portion of the cycle, but even in these partial-stall cases, considerable hysteresis in C_N and C_M vs α was observed.

Although the vortex-shedding phenomenon appears to be a general feature of all oscillating airfoils over a wide range of Reynolds numbers, significant differences in the dynamic force and moment characteristics were observed on different airfoils. This suggests that future improvements in airfoil design would be possible if dynamic stall were better understood theoretically.

References

[1] Ham, N.D. and Garelick, M.S., "Dynamic Stall Considerations in Helicopter Rotors," *Journal of the American Helicopter Society*, Vol. 13, April 1968, pp. 49-55.

[2] Ham, N.D., "Aerodynamic Loading on a Two-Dimensional Airfoil during Dynamic Stall." *AIAA Journal*, Vol. 6, Oct. 1968, pp. 1927-1934.

[3] Werlé, H., "Visualization Hydrodynamique d'Ecoulements Instationnaires," *Proceedings of the IUTAM Symposium on Recent Research on Unsteady Boundary Layers*, Quebec, Canada, 1971.

[4] Philippe, J.J. and Sagner, M., "Calcul et Mésure des Forces Aérodynamiques sur un Profil Oscillant avec et sans Décrochage," *Agard Conference Proceedings No. 111 on Aerodynamics of Rotary Wings*, Paper 11, Sept. 1972.

[5]Martin, J.M., Empey, R.W., McCroskey, W.J., and Caradonna, F.X., "An Experimental Analysis of Dynamic Stall on an Oscillating Airfoil," *Journal of the American Helicopter Society,* Vol. 19, Jan. 1974, pp. 26-32.

[6]Ruiter, G.H., Nagib, A.M., and Fejer, A.A., "Visualization of Unsteady Flow over Oscillating Airfoils," *Proceedings of Second Symposium on Turbulent Measurements in Liquids*, Rolla, Mo. 1971.

[7]Silcox, R.J. and Szwarc, W.J., "Wind-Tunnel Dynamic Analysis of an Oscillating Airfoil," AIAA Paper 74-259, Washington, D.C., 1974.

[8]Johnson, W. and Ham, N.D., "On the Mechanism of Dynamic Stall," *Journal of the American Helicopter Society*, Vol. 17, Oct. 1972, pp. 36-45.

[9]Crimi, P. and Reeves, B.L., "A Method for Analyzing Dynamic Stall," NASA CR-2009, May 1972; also AIAA Paper 72-37, and AGARDograph No. 172, 1973.

[10]Lang, J.D., "On Predicting Leading-Edge Bubble Bursting on an Airfoil in Unsteady Incompressible Flow," Memo 109, 1973, Cranfield Inst. of Technology, Cranfield, England.

[11]Baudu, N., Sagner, M., and Souquet, J., "Modelisation du Décrochage Dynamique d'un Profil Oscillant," *AAAF 10th Colloque d'Aérodynamique Appliquée*, Lille, France, Nov. 1973.

[12]McCroskey, W.J., Carr, L.W., and McAlister, K.W., "Dynamic Stall Experiments on Oscillating Airfoils," AIAA Paper 75-125, Pasadena, Calif., 1975.

[13]McCroskey, W.J. and Philippe, J.J., "Unsteady Viscous Flow on Oscillating Airfoils," *AIAA Journal*, Vol. 13, Jan. 1975, pp. 71-79.

[14]Soderman, P.T., "Aerodynamic Effects of Leading-Edge Serrations on a Two-Dimensional Airfoil," NASA TM X-2643, Sept. 1972.

[15]Schwind, R.G. and Allen, H.J., "The Effects of Leading-Edge Serrations on Reducing Flow Unsteadiness about Airfoils," AIAA Paper 73-89, Washington, D.C., Jan. 1973; also NACA CR-2344, 1972.

[16]Sandborn, V.A. and Kline, S.J., "Flow Models in Boundary-Layer Stall Inception," *ASME Transactions, Series D-Journal of Basic Engineering*, Vol. 83, 1961, pp. 317-327.

[17]Gault, D.E., "A Correlation of Low-Speed Airfoil Section Stalling Characteristics with Reynolds Number and Airfoil Geometry," NACA TN 3963, March 1956.

[18]McCullough, G.B. and Gault, D.B., "Examples of Three Representative Types of Airfoil-Section Stall at Low Speed," NACA TN 2502, Sept. 1951.

[19]Gregory, N. and O'Reilly, C.L., "Low-Speed Aerodynamic Characteristics of NACA 0012 Airfoil Section, Including the Effects of Upper-Surface Roughness Simulating Hoar Frost," Aero Rept. 1308, Jan. 1970, National Physical Lab., Teddington, England.

[20]Ridder, S.O., "Experimental Studies of the Leading-Edge Suction Force, Including the Maximum Attainable Suction Force versus Reynolds Number and the Induced Distributions on Various Wing Planforms and Air Intakes," *Ninth ICAS Congress*, Paper 74-47, Haifa, Israel, Aug. 1974.

[21]Wallis, R.A., "Boundary-Layer Transition at the Leading Edge of Thin Wings and Its Effect on General Nose Separation," *Advances in Aeronautical Science*, Vol. 3, Pergamon Press, New York, 1962, pp. 161-184.

[22]Evans, W.T. and Mort, K.W., "Analysis of Computed Flow Parameters for a Set of Sudden Stalls in Low-Speed Two-Dimensional Flow," NASA TN D-85, Aug. 1959.